Physica A 438 (2015) 424–435

Contents lists available at ScienceDirect

Physica A

journal homepage: www.elsevier.com/locate/physa

A cellular automata model of Ebola virus dynamics

Emily Burkhead [a,1], Jane Hawkins [b,*]

[a] Department of Mathematics and Computer Science, Meredith College, United States

[b] Department of Mathematics, University of North Carolina at Chapel Hill, CB #3250, Chapel Hill, NC 27599-3250, United States

HIGHLIGHTS

- We construct a stochastic cellular automaton model for the Ebola virus.
- Basic dynamical rules governing viral spread are adapted to the Ebola setting.
- Rigorous results are given about the dynamics.
- Model output simulates the timeline of the infection and captures fatality rates.

ARTICLE INFO

Article history:
Received 2 June 2015
Available online 15 July 2015

Keywords:
Ebola
Cellular automata
Virus spread

ABSTRACT

We construct a stochastic cellular automaton (SCA) model for the spread of the Ebola virus (EBOV). We make substantial modifications to an existing SCA model used for HIV, introduced by others and studied by the authors. We give a rigorous analysis of the similarities between models due to the spread of virus and the typical immune response to it, and the differences which reflect the drastically different timing of the course of EBOV. We demonstrate output from the model and compare it with clinical data.

1. Introduction

Ebola virus (EBOV) is a filovirus that causes severe illness in most humans who are exposed to it. A filovirus is a negative, single-stranded RNA virus whose genome is configured linearly, which differs from a retrovirus such as HIV (human immunodeficiency virus) in its method of replication [1,2]. On the other hand, similarities between these two types of viruses, especially in terms of their negative effect on the immune system, have been studied for some time [3]. In October of 2014 the World Health Organization (WHO) Ebola Response Team published a report estimating the fatality rate of Ebola Virus Disease (EVD) to be around 70.8% [4], but hospitalized patients during the recent outbreak in West Africa had a slightly lower fatality rate. Due to the difficulty in gathering accurate data, differences among patient care, and individual responses to treatment, there is a wide range of fatality rates reported, from 25% to 90% [5].

Because of the extreme virulence of EBOV, autopsies and handling of fluids of infected patients are limited and avoided when possible [5], making mathematical and computer models of the disease a particularly valuable tool. In Ref. [6], a computer model first introduced in 2001 by Zorzenon dos Santos and others [7] for HIV, was amended and studied rigorously to show precisely which viral dynamics were being modeled, how the set of infected cells spreads, and how immune response and drug therapy affects the dynamics. The authors of Ref. [6] extracted some results that apply independently

* Corresponding author.
E-mail addresses: burkhead@unc.edu (E. Burkhead), jmh@math.unc.edu (J. Hawkins).
[1] Current address: Department of Mathematics, University of North Carolina at Chapel Hill, CB #3250, Chapel Hill, NC 27599-3250, United States.

http://dx.doi.org/10.1016/j.physa.2015.06.049
0378-4371/

of the virus in question and showed how varying parameters changed the model. The spread of HIV, as well as the effect of administering drugs, has been modeled by SCAs (see for example, Refs. [6,8–10] and references therein). In Refs. [11,10] the later chronic stages of viral infection were isolated from the model and studied further; these studies involved Markov processes reflecting randomness in the development and control of a chronic viral condition. The EBOV time scale is much shorter and there seems to be no chronic residual disease that has been observed in survivors of the acute illness up to now. Therefore the early viral dynamics control the progression and outcome. In this paper we adapt the early stages of the viral dynamics model in Ref. [6] to EBOV.

A cellular automaton (CA) model is an agent-based model, a computer simulation of the process of the viral spread in an organ based on simple rules. For example, a rule that all viral models have in common is that if a cell is contiguous to an actively infected cell, it becomes infected in the next time step. An SCA uses a small number of simple rules chosen randomly using data-based probabilities, to emulate differences in immune responses to viral spread. By running an SCA simulation, we achieve a variety of outcomes from a single model.

In this paper, we modify the original (HIV) SCA model to use parameters and cellular automata rules specific to the spread of EBOV within an individual organ. While much is still unknown about EBOV, we can use features of existing models for the general properties of viral spread and the body's typical immune response to it. We change some of the salient features of the HIV model as needed for this setting. As of this writing, it is believed that viral mutation occurs much less with EBOV than with HIV though the possibility that EBOV mutations might affect future diagnosis and treatment is being studied [12]. In contrast, it has been known for some time that HIV shows extensive genetic variation even within individual hosts, making HIV one of the fastest evolving of all organisms [13]. Therefore, one of the main modifications we make is to remove the rule leading to viral reservoirs due to mutating viruses, a characteristic property of HIV. We eliminate that as a mathematically possible rule and replace it with a rule that reflects a delayed or slower immune response to the virus. The rest of the rules in the SCA stay the same and this small change immediately speeds up the course of the viral infection to a fairly rapid recovery or death.

The paper is organized as follows. In Section 2 we give the basic definitions of CAs and SCAs, introduce the rules used in our model of EBOV dynamics, and present theoretical results. The output obtained by various computer simulations utilizing different parameters is analyzed in Section 3, and we discuss some conclusions in Section 4.

2. Theory of cellular automata models

2.1. Cellular automata

Let $\mathcal{A}$ denote the finite state space or *alphabet*, $\mathcal{A} = \{0, 1, 2, 3\}$. We use state 0 to represent a healthy cell site in an organ, and states 1 and 2 to represent infectious cells able to infect neighboring cells. State 3 represents a depleted (dead) cell site. Then, we define the integer lattice $\mathbb{Z}^2 = \{\vec{\imath} = (i, j),\ i, j \in \mathbb{Z}\}$, viewed as a subset in the plane (or on a surface, by identifying edges of a polygon). The length of a vector in $\mathbb{Z}^2$ is taken as $\|\vec{\imath}\| = \max\{|i|, |j|\}$. The space on which a cellular automaton acts is $X = \mathcal{A}^{\mathbb{Z}^2}$, which we think of as the integer lattice $\mathbb{Z}^2$ in the plane with exactly one value from the state space $\mathcal{A}$ placed at each coordinate (i, j) in the lattice. The space X is mathematically equivalent to the set of functions from $\mathbb{Z}^2$ to $\mathcal{A}$. So, for each $x \in X$ and $\vec{\imath} = (i, j) \in \mathbb{Z}^2$ we write $x_{(i,j)}$ to denote *the coordinate of x at* $\vec{\imath}$, with $x_{(i,j)} \in \{0, 1, 2, 3\}$. Similarly for any finite set $E \subseteq \mathbb{Z}^2$, we define x_E to be the block of coordinates $\{x_{\vec{\imath}} : \vec{\imath} \in E\}$; i.e., $x_E \in \mathcal{A}^{|E|}$ where $|E|$ is the cardinality of E.

We make X into a compact space by using the classical metric on X, which is defined so that two points are close if their coordinates agree on a large central region. First, we define a neighborhood of radius $k \in \mathbb{N} \cup \{0\}$ about $(0, 0) \in \mathbb{Z}^2$, by $N_k = \{\vec{\imath} = (i, j) : |i|, |j| \leq k\} = \{\vec{\imath} : \|\vec{\imath}\| \leq k\}$. Then, *the metric* d_X *on* X is defined as follows: for any pair of points $x, v \in X$, $d_X(x, v) = \frac{1}{2^k}$ where $k = \min\left\{m : x_{N_m} \neq v_{N_m}\right\}$. We call a *pattern* any fixed $(2k + 1)^2$ square block of states from $\mathcal{A}$ (or a finite union of $(2k + 1)^2$ square blocks), $k \in \mathbb{N}$. We form a basis for the metric topology from the following collection of sets. For any pattern u, define $B_u = \{x \in X : x_{N_k} = u\}$ to be the *u-cylinder of radius k* (centered at $(0, 0)$). B_u is precisely the set of points from X whose central block of coordinates extending out k units in each direction from $(0, 0)$ coincides with the fixed pattern u.

The space X provides a model for an organ that is susceptible to the virus such as liver, spleen, lungs, or skin [5,14]. Each point $x \in X$ represents a configuration of the healthy, infected, and depleted cells of the organ at any given time, and each coordinate $x_{(i,j)}$ shows the state of the organ at that location where a coordinate is either a cell or a site of cells, depending on the organ. In order to dynamically move around within an organ and sample the state at any location, we define the *shift maps on* X as follows:

$$\forall \vec{\imath} = (i, j) \in \mathbb{Z}^2, \quad [\sigma_{\vec{\imath}}(x)]_{(k,l)} = x_{(i+k,j+l)}.$$

With respect to the metric d_X, each shift $\sigma_{\vec{\imath}}$ is a continuous transformation on X. With all this structure in place, we are now able to define a CA.

Definition 2.1. A **2-dimensional cellular automaton (CA)** is a continuous transformation F on X such that for every $\vec{\imath} \in \mathbb{Z}^2$, $F \circ \sigma_{\vec{\imath}} = \sigma_{\vec{\imath}} \circ F$.

It is well-known that each CA is characterized by a local rule (of radius $r \geq 0$), based on the definition of continuity in the metric topology on X. In the next theorem this is made precise.

Theorem 2.2 ([15]). *The map $F : X \to X$ is a CA if and only if there exists an integer $r \geq 0$ and a map $f : \mathcal{A}^{(2r+1)^2} \to \mathcal{A}$ such that for every $x \in X$,*

$$F(x)_{\vec{i}} = f(x_{N_r+\vec{i}}). \tag{2.1}$$

The map f that appears in (2.1) is called the *local rule* for the CA F as f describes the CA completely.

It is useful to regard a CA as a map or rule that updates each coordinate in X at each time step by looking only at finitely many nearby coordinates. If F is a CA, we iterate F using the notation $F^k(x) = F \circ \cdots \circ F(x)$ to denote composition with itself k times.

An analogous space X could be defined to be the set of functions from $\mathbb{Z}^d$ to $\mathcal{A}$ for any integer dimension $d \geq 1$. We find, however, that using two dimensions captures most of the EBOV dynamics that are understood so far. The SCA model of the spread of the virus we define below does not depend on the dimension of the organ, but rather on the relative positions of cells to each other. Moreover, the actual viral spread could take place in one-dimensional channels (narrow capillaries), along two-dimensional sheets (such as the skin), and in 3-dimensional organs (for example, the liver) [5]. All of the math analysis that follows can be done for arbitrary dimension d as well. However using $d = 2$ makes the concepts and notation easier to explain in this paper.

2.2. CAs model the immune response to Ebola

We use three different 2-dimensional CAs to model the immune response to viruses such as Ebola, combining them into a stochastic cellular automaton (SCA) in Section 2.3. Here, we introduce them independently.

In a healthy individual with a functioning immune system, infected cells die quickly and are replenished by healthy ones, while at the same time the infected cells are also infectious, able to infect nearby healthy cells. The CA Q models this quick response: all infectious cells are depleted in a single time step, as we see in local rule q which has radius 1. On the state space $\mathcal{A} = \{0, 1, 2, 3\}$, define the local rule $q : \mathcal{A}^{3\times 3} \to A$ as follows:

$$q\begin{pmatrix} * & * & * \\ * & 0 & * \\ * & * & * \end{pmatrix} = \begin{cases} 1 & \text{if at least one } {}^* \text{ is 1 or 2} \\ 0 & \text{otherwise,} \end{cases}$$

$$q\begin{pmatrix} * & * & * \\ * & a & * \\ * & * & * \end{pmatrix} = 3 \quad \text{for } 1 \leq a \leq 2,$$

$$q\begin{pmatrix} * & * & * \\ * & 3 & * \\ * & * & * \end{pmatrix} = 0.$$

The dynamics of Q are illustrated in Fig. 1. White represents 0, healthy cells, and black represents 3, depleted (dead) cells; pink represents state 1, the initial infection, as shown in the first frame. State 2 does not appear under iteration of Q when we begin with an initial point consisting of 0s and 1s. Above each frame is the time step, where one time increment corresponds to one day. As shown, initial infection spreads and then clears out, with a return to the all healthy configuration in a very short time frame. The timing to clear out the infection depends on the number and proximity of initial 1s; fewer and farther spaced out 1s will require a longer time to return to the all 0 configuration.

We use two small variations on this CA to model what happens if the immune system is compromised or simply delayed in its response. We call these CAs L for longer response and D for depleted response; we define them by their radius $r = 1$ local rules, ℓ and d, respectively. For the longer response, an additional timestep will be needed for the immune system to wipe out an initially infected site (1 passes to 2 and then to 3). The depleted response is so named because a dead site will stay dead (3 stays 3). All other portions of the rules are the same as in the quick response. So, we define the local rules $\ell, d : \mathcal{A}^{3\times 3} \to \mathcal{A}$ by:

$$d\begin{pmatrix} * & * & * \\ * & a & * \\ * & * & * \end{pmatrix} = q\begin{pmatrix} * & * & * \\ * & a & * \\ * & * & * \end{pmatrix} \quad \text{for any } a \neq 3, \text{ while } d\begin{pmatrix} * & * & * \\ * & 3 & * \\ * & * & * \end{pmatrix} = 3;$$

$$\ell\begin{pmatrix} * & * & * \\ * & 0 & * \\ * & * & * \end{pmatrix} = q\begin{pmatrix} * & * & * \\ * & 0 & * \\ * & * & * \end{pmatrix}; \quad \text{for any } a \neq 0, \ \ell\begin{pmatrix} * & * & * \\ * & a & * \\ * & * & * \end{pmatrix} = a + 1 \pmod 3.$$

The dynamics of L are virtually identical to those of Q and are shown in Fig. 2. We see the appearance of state 2, represented by teal; initial infection once again spreads and then clears out. The dynamics of D are shown in Fig. 3. Instead of recovery, we see that the infection eventually depletes all cells.

These three rules are variations on those used in the study HIV [6]. Our L and D parallel two of the three rules in the HIV model, however we use fewer total states (four here as compared to seven for the HIV model) since EBOV progresses much more quickly than does HIV. The third rule used in the HIV model took into account the very fast mutation rate of the virus.

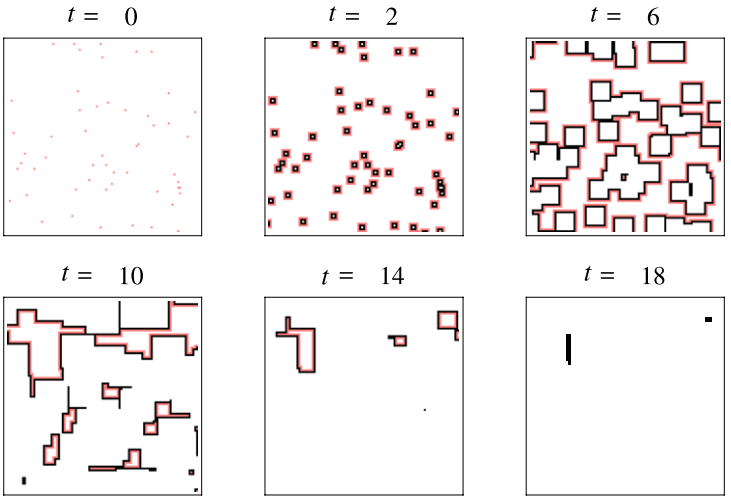

Fig. 1. Iteration of Q: infection spreads, then clears out.

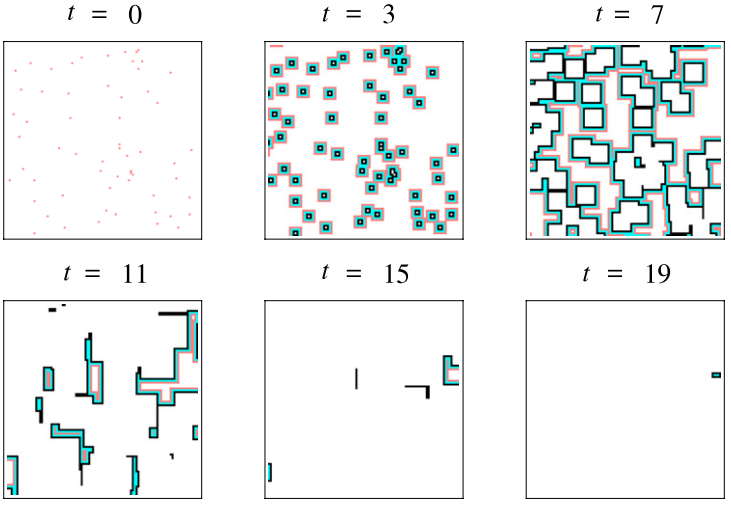

Fig. 2. Iteration of L: infection spreads, then clears out.

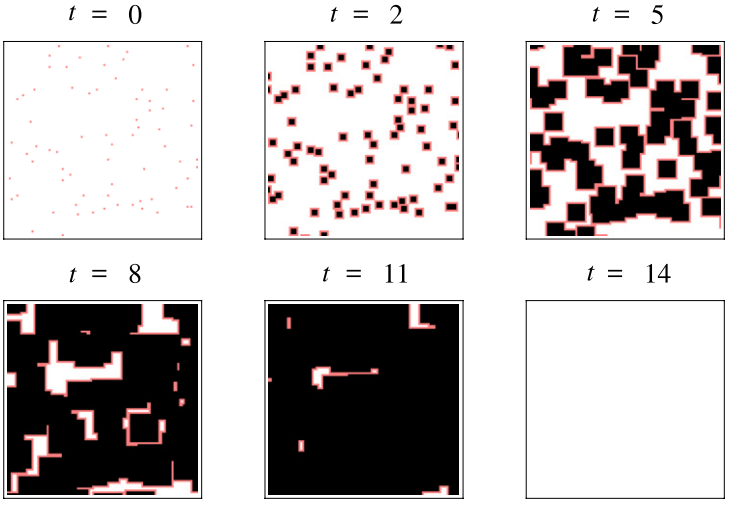

Fig. 3. Iteration of D: infection spreads, resulting in cell death.

Despite the likelihood that EBOV might mutate due to transcription errors based on its RNA replication [12], it seems that the genetic sequence of EBOV is relatively stable [2]. Our motivation for using both Q and L comes from observations that antibody responses are very different for patients who survive the disease when compared to those who have lethal cases; "deceased patients show a lower or even absent antibody response [1]".

Formal statements regarding the dynamics of each of Q, L, and D are treated next. Many of the results correspond to ones stated and proven for the CAs considered in the HIV model in Ref. [6]. Rather than provide a complete proof of our results here, then, we simply indicate the differences needed to modify the proofs from Ref. [6].

Proposition 2.3. *Let $\overline{0} \in X$ be such that $\overline{0}_{(i_1,i_2)} = 0$ for all $(i_1, i_2) \in \mathbb{Z}^2$. Then $\overline{0}$ is a fixed point under each of the CAs Q, L, and D.*

Physically, this would correspond to a completely healthy organ: with no infection in any site, the organ simply stays completely healthy for all time. The proof is obvious: since none of the 0 states are adjacent to any 1s or 2s, they will all update to 0 under iteration of each of the three CAs.

There are points in X arbitrarily close to this fixed point which have drastically different trajectories; $\overline{0}$ is not what is called a point of equicontinuity. A point $x \in X$ is a *point of equicontinuity* for a transformation F if for any $\varepsilon > 0$, there exists $\delta > 0$ so that any $y \in X$ having $d_X(x, y) < \delta$ has $d_X(F^n x, F^n y) < \varepsilon$ for all $n \geq 0$.

Proposition 2.4. *$\overline{0}$ is not a point of equicontinuity for Q, L, or D.*

Proof. The proof of Proposition 4.1 in Ref. [6] can be applied here due to the similar mechanism by which $0 \mapsto 1$ in the local rules of the CAs. □

In our model, we are primarily considering initial points which consist strictly of states 0 and 1. All of these initial points converge under iteration of both Q and L to the fixed point $\overline{0}$, which is to say that these two CAs model a successful immune response to an ordinary virus. Under iteration of D, our initial points all converge to $\overline{3}$ and they are points of equicontinuity.

Proposition 2.5. *Let $x \in X$ have $x_{(i_1,i_2)} \in \{0, 1\}$ for all $(i_1, i_2) \in \mathbb{Z}^2$. Then $\{Q^n x\} \to \overline{0}$, $\{L^n x\} \to \overline{0}$, and $\{D^n x\} \to \overline{3}$ as $n \to \infty$.*

Proposition 2.6. *Let $x \in X$ have $x_{(i_1,i_2)} \in \{0, 1\}$ for all $(i_1, i_2) \in \mathbb{Z}^2$ but $x \neq \overline{0}$. Then, x is a point of equicontinuity for D.*

Proof. The proof of each of these statements is obtained in a virtually identical manner to that of the CAs considered in Refs. [6, Propositions 4.3, 4.4, and 4.5]. The only difference is that the number of iterates needed for convergence is slightly less here since we have fewer states in the alphabet $\mathcal{A}$. □

Although the orbits of our initial points are certain under all three CAs, there are other points arbitrarily close to a given initial point of 0s and 1s which have drastically different orbits under both Q and L, giving rise to some unpredictability. It is unfortunate, then, that these are the two CAs which bring our initial points to a good outcome, with all healthy sites; D takes our initial points to a very bad outcome, where all sites are dead. Once again, we can turn to the proof of a similar result that appears in Ref. [6, Proposition 4.7], which relies on the presence of a fully blocking pattern. A *fully blocking pattern* is a finite arrangement of states from the alphabet whose appearance in a point determines the states at those coordinates for all subsequent iterations of a CA, regardless of what states occur nearby.

Proposition 2.7. *Let $x \in X$ have $x_{(i_1,i_2)} \in \{0, 1\}$ for all $(i_1, i_2) \in \mathbb{Z}^2$. Then x is not a point of equicontinuity for Q or for L.*

Proof. Since the fully blocking pattern given in Ref. [6], consisting of concentric rings of 0s, 2s, and 0s, also happens to be a fully blocking pattern for our L, as shown in Fig. 4, the proof of Ref. [6] extends with only minor modifications to L.

Although the concentric rings of 0s and 2s turn out not to be fully blocking for Q, we are still able to utilize the aforementioned proof for Q by utilizing a different fully blocking pattern, the one in Fig. 5, in much the same way. □

By a result of Ref. [16], we can also use these fully blocking patterns to create many initial points in X which do have predictable orbits under each of the three CAs. We define a CA to be *almost equicontinuous* if its set of equicontinuity points contains a countable intersection of dense open sets.

Proposition 2.8. *The CAs Q, L, and D are each almost equicontinuous.*

Proof. The pattern of Fig. 5 is fully blocking for Q. The pattern of Fig. 4 is fully blocking for L. The pattern $\begin{matrix} 3 & 3 & 3 \\ 3 & 3 & 3 \\ 3 & 3 & 3 \end{matrix}$ is fixed under D and therefore fully blocking for D. Thus, we can apply Theorem 6.3 of Ref. [16] to each of Q, L, and D to conclude that these three CAs are each almost equicontinuous. □

2.3. Stochastic cellular automata

Now, we combine the three CAs above to form a stochastic cellular automaton (SCA). The idea is that in each iteration, we will independently choose which of these CAs to apply at each site in the lattice. The choices need not be equally weighted,

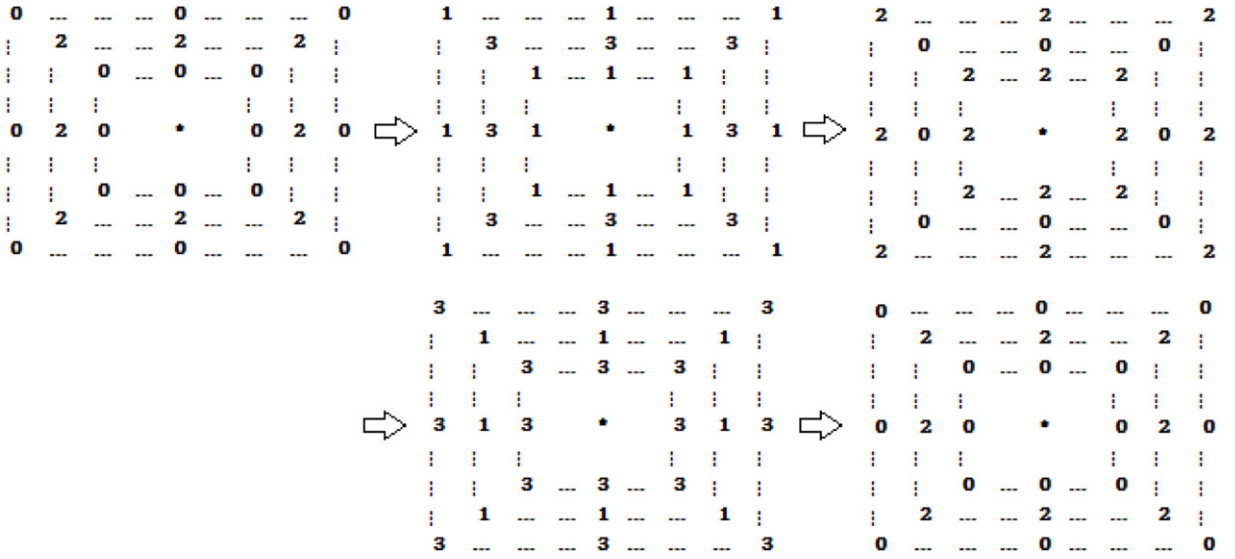

Fig. 4. A fully blocking pattern for L; the pattern reappears after four iterations.

$$\begin{matrix} 1&1&3 \\ 3&0&3 \\ 3&1&1 \end{matrix} \mapsto \begin{matrix} 3&3&0 \\ 0&1&0 \\ 0&3&3 \end{matrix} \mapsto \begin{matrix} 0&0&1 \\ 1&3&1 \\ 1&0&0 \end{matrix} \mapsto \begin{matrix} 1&1&3 \\ 3&0&3 \\ 3&1&1 \end{matrix}$$

Fig. 5. A fully blocking pattern for Q: the pattern reappears after three iterations.

but the probability of making each choice is consistent across all coordinates. Since we have three CAs, we let $\mathcal{C} = \{1, 2, 3\}$ be an index set. The local rule for the SCA will then need to take as arguments both a single element of $\mathcal{C}$ as well as a 3×3 block of symbols from A. To iterate the SCA, we will need to select one rule for each time step. Thus, we let $\Omega = \mathcal{C}^{\mathbb{N}\cup\{0\}}$ model the random selection at a single site. The shift space Ω is equipped with the standard metric $d_\Omega(\omega, \zeta) = \frac{1}{2^k}$, where $k = \min\{m \in \mathbb{N} \cup \{0\} : \omega_m \neq \zeta_m\}$ as well as the standard shift map s given by

$$[s(\omega)]_n = \omega_{n+1}. \tag{2.2}$$

For convenience of notation, we will rename $F_1 = Q$, $F_2 = L$, and $F_3 = D$, with corresponding local rules $f_1 = q$, $f_2 = \ell$, and $f_3 = d$. Constructing an SCA begins with a local rule. On the space $\Omega \times \mathcal{A}^{3\times 3}$, define

$$g(\omega, u) = f_{\omega_0}(u) = \pi_{\mathcal{A}}\left(s(\omega), f_{\omega_0}(u)\right), \tag{2.3}$$

where $\pi_{\mathcal{A}}$ denotes projection onto the second coordinate (which is in $\mathcal{A}$).
Then, each choice of $\overline{\omega} = \prod_{(i,j)\in\mathbb{Z}^2} \omega^{(i,j)} \in \prod_{(i,j)\in\mathbb{Z}^2} \Omega = \overline{\Omega}$ will define a mapping $F_{\overline{\omega}} : \mathcal{A}^{\mathbb{Z}^2} \to \mathcal{A}^{\mathbb{Z}^2}$ given by

$$[F_{\overline{\omega}}(x)]_{(i,j)} = g\left(\omega^{(i,j)}, x_{N_1}\right) = f_{\omega_0^{(i,j)}}\left(x_{N_1}\right). \tag{2.4}$$

We denote the SCA by $F_{\overline{\Omega}}$. To iterate $F_{\overline{\Omega}}$, we need to shift each one-sided sequence $\omega^{(i,j)}$ simultaneously. Let $\overline{s} : \overline{\Omega} \to \overline{\Omega}$ be the shift mapping that performs the shift of (2.2) coordinate-wise, that is,

$$[\overline{s}(\overline{\omega})]_n^{(i,j)} = \left[s(\omega^{(i,j)})\right]_n = \left[\omega^{(i,j)}\right]_{n+1}. \tag{2.5}$$

Now we find the tth iterate of $F_{\overline{\Omega}}$ by computing, for each fixed pair $(\overline{\omega}, x) \in \overline{\Omega} \times X$,

$$F_{\overline{\omega}}^t(x) = F_{\overline{s}^{t-1}\overline{\omega}} \circ \cdots \circ F_{\overline{s}\overline{\omega}} \circ F_{\overline{\omega}}(x). \tag{2.6}$$

Although $F_{\overline{\Omega}}$ is not a true CA, there is a continuous shift-commuting mapping, $\overline{F} : Y = (\Omega \times \mathcal{A})^{\mathbb{Z}^2} \to Y$, which represents $F_{\overline{\Omega}}$. Further, we define properties such as equicontinuity for $F_{\overline{\Omega}}$ using $\overline{F}$. See Ref. [6] for further details of the general construction.

The probability of choosing each CA, F_1, F_2, or F_3 (at each coordinate and at each time step) is governed by a probability vector, $\rho = (\rho_1, \rho_2, \rho_3)$. That is, all $\rho_k \geq 0$ and $\sum_{k=1}^3 \rho_k = 1$. This vector defines an independent identically distributed measure μ on Ω, the usual Bernoulli measure on Ω determined by ρ, which is given by the following: for each finite sequence $c_0, c_1, \ldots, c_m$, we have $\mu(\{\omega \in \Omega : \omega_k = c_k \text{ for } k = 0 \cdots m\}) = \rho_{c_0} \cdot \rho_{c_1} \cdots \rho_{c_m}$. The measure μ is invariant under the shift s. Using this measure coordinate-wise on each copy of Ω, we obtain the canonical probability product measure $\overline{\mu}$ on $\overline{\Omega}$ preserved by $\overline{s}$. More can be said about the measures μ and $\overline{\mu}$; see Ref. [6] for further details.

We next study the behavior of initial points consisting of just 0s and 1s under our SCA. Illustrations of the dynamics are shown in Section 3. Theorems 2.10 and 2.11 give statements of the long-term behavior of the SCA. Each of the two proofs relies on Lemma 2.9, which is stated next. As with the SCA which modeled HIV progression, blocks of healthy coordinates do not persist under iteration of the EBOV SCA. Initial points consisting of 0s and 1s (that are not completely healthy) will eventually see some infection in every site.

Lemma 2.9. *Let $x \in \{0,1\}^{\mathbb{Z}^2} \subseteq X$ but $x \neq \overline{0}$. Given an integer $k > 0$, let $N_k = \{(i,j) : |i|, |j| \leq k\} \subseteq \mathbb{Z}^2$ be the neighborhood of radius k about $(0,0) \in \mathbb{Z}^2$, and let $T = \min\{\|(l,m) - N_k\| : x_{(l,m)} = 1\}$ be the minimum distance a value 1 is to the neighborhood N_k. Then for each $(i,j) \in N_k$ and each $c \in \{1,2,3\}$, $(F_c^t x)_{(i,j)} = 1$ for some $t \leq (T + 2k)$.*

Proof. The proof of Lemma 4.2 in Ref. [6] applies here without any changes, due to the similar mechanism by which 0 updates to 1 under all the CAs being considered. □

When only the quick and depleted CAs are in play, we expect a full recovery in the long run. In Theorem 2.10, we show that all initial points consisting only of 0 and 1 states will almost surely converge to the point $\overline{0}$.

Theorem 2.10. *When $\rho_2 = 0$, any $x \in \{0,1\}^{\mathbb{Z}^2}$ has $\lim_{n\to\infty} F_{\overline{\omega}}^n x = \overline{0}$ for $\overline{\mu}$-almost every $\overline{\omega} \in \overline{\Omega}$.*

Proof. Let $\varepsilon = 2^{-k} > 0$ and let $x \in \{0,1\}^{\mathbb{Z}^2}$. For each $(i,j) \in \mathbb{Z}^2$, take any $\omega^{(i,j)} \in \{1,3\}^{\mathbb{N}\cup\{0\}}$, with $\overline{\omega} = \prod_{(i,j)\in\mathbb{Z}^2} \omega^{(i,j)}$.

Since $\overline{0}$ is fixed for the SCA, we assume $x \neq \overline{0}$. Let N_k be the k-neighborhood of $(0,0) \in \mathbb{Z}^2$ and let $T \geq 0$ be the distance from N_k to the nearest 1 in x, as in the statement of Lemma 2.9. Since both Q and D update state 0 to state 1 under exactly the same conditions, then at each $(i,j) \in \mathbb{Z}^2$, we will have $\left(F_{\overline{\omega}}^{t_{(i,j)}} x\right)_{(i,j)} = 1$ for some $t_{(i,j)} \leq T + 2k$, similar to the statement of Lemma 2.9. Then $\left(F_{\overline{\omega}}^{t_{(i,j)}+1} x\right)_{(i,j)} = 3$ since both Q and D update all 1s to 3s, and $\left(F_{\overline{\omega}}^{t_{(i,j)}+2} x\right)_{(i,j)} \in \{0,3\}$, with the specific value dependent on whether $\omega^{(i,j)}_{t_{(i,j)}+2}$ is 1 or is 3. Any 0s that appear as $\left(F_{\overline{\omega}}^n x\right)_{(i,j)}$ for some $(i,j) \in N_k$ and some $n \geq t_{(i,j)} + 2$ will therefore be adjacent only to other 0s and 3s, and thus, will stay in state 0 for all iterates beyond n as well. The only way a coordinate $(i,j) \in N_k$ will not eventually become a perpetual 0 is that $\omega_n^{(i,j)}$ must be 3 for all $n \geq t_{(i,j)}$. Define

$$W = \left\{ \overline{\omega} = \prod_{(i,j)\in\mathbb{Z}^2} \omega^{(i,j)} \in \overline{\Omega} : \exists (i,j) \in N_k \text{ such that } \omega_n^{(i,j)} = 3 \ \forall n \geq t_{(i,j)} + 2 \right\}.$$

We have shown above, then, that for any $\overline{\omega} \notin W$, $\lim_{n\to\infty} F_{\overline{\omega}}^n x = \overline{0}$; we next show that W has measure 0 in $\overline{\Omega}$. First, note that W is the finite union of an intersection of cylinder sets, $W = \bigcup_{(i,j)\in N_k} \bigcap_{m=1}^{\infty} s^{(t_{(i,j)}+2)} \left(B_{[3^m]}\right)$, where 3^m indicates the concatenation of 3 with itself $m \geq 1$ times, and $s^{(t_{(i,j)}+2)}$ shifts to where the infinite string of 3s begins.

$$\begin{aligned}
\overline{\mu}(W) &= \overline{\mu}\left(\bigcup_{(i,j)\in N_k} \bigcap_{m=1}^{\infty} s^{(t_{(i,j)}+2)} \left(B_{[3^m]}\right) \right) \\
&= \prod_{(i,j)\in N_k} \mu\left(\bigcap_{m=1}^{\infty} s^{(t_{(i,j)}+2)} \left(B_{[3^m]}\right) \right) \\
&= \prod_{(i,j)\in N_k} \lim_{m\to\infty} \mu\left(s^{(t_{(i,j)}+2)} \left(B_{[3^m]}\right) \right), \quad \text{as the cylinder sets are nested} \\
&= \prod_{(i,j)\in N_k} \lim_{m\to\infty} \mu\left(B_{[3^m]}\right), \quad \text{as } \mu \text{ is invariant under } s \\
&= \prod_{(i,j)\in N_k} \lim_{m\to\infty} (\rho_3)^m \\
&= \prod_{(i,j)\in N_k} 0, \quad \text{as } 0 < \rho_3 < 1 \\
&= 0.
\end{aligned}$$

Therefore, $\lim_{n\to\infty} F_{\overline{\omega}}^n x = \overline{0}$ for $\overline{\omega}$ in a set of $\overline{\mu}$ measure 1. □

Despite there being some predictability in the CAs Q, L, and D individually, and the existence of the same fully blocking pattern for each CA, since the pattern has a different trajectory under each CA, we cannot combine the results of Proposition 2.8 to guarantee equicontinuity points for the stochastic CA. In fact, there are no points of equicontinuity in $F_{\overline{\omega}}$, regardless of which choice of $\overline{\omega}$ is made.

Theorem 2.11. *The SCA generated by Q, S, and D does not have any points of equicontinuity.*

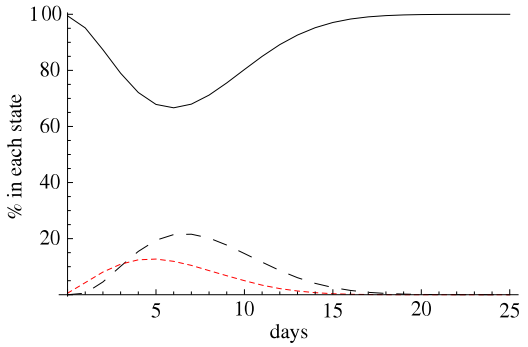

Fig. 6. We proved that when $\rho_2 = 0$, for every initial infection, recovery is almost certain. Here $\rho_3 = 0.45$.

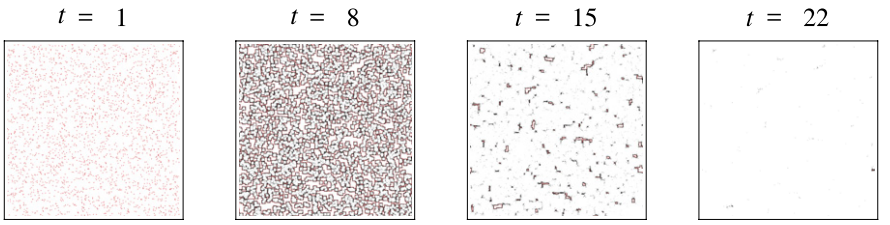

Fig. 7. This shows the SCA output illustrating Theorem 2.10 using the parameters from Fig. 6.

Proof. The proof is identical to the one of Theorem 4.9 in Ref. [6] with a minor change of replacing the depleted (dead) state of 6 in Ref. [6] with the depleted (dead) state of 3 here. □

3. Results

In this section we show the outcome of running the SCA model for EBOV with a variety of parameter choices for ρ_1, ρ_2, and ρ_3, the probabilities that the rules for Q, L, and D respectively are applied at each site and each time step. A time step here represents approximately one day, and recall that the space X represents an organ that is susceptible to the virus such as liver, spleen, lungs, or endothelial cells [14]. Our algorithms are implemented on a 700×700 2-dimensional grid using Mathematica.

3.1. The Ebola model parameters

We run the model using a variety of parameters. While it is known that there is some correlation between the viral load and the prognosis for humans affected with Ebola hemorrhagic fever (EHF), a frequent rapid consequence of infection by EBOV [14], the initial viral load is difficult to determine. More precisely, the initial percentage of infected cells once EBOV is introduced into the organ has not been determined. We therefore typically use the initial load for HIV as a substitute since that range is known (see Ref. [6] and references therein). The initial viral proportion for HIV is $(10^{-2} + 10^{-3})/2 = 0.0055$; however the model is flexible enough that this parameter can be changed as data becomes available.

When an otherwise healthy person is infected with EBOV, each of the rules Q and L model a successful immune response. We use the rule L with a low percentage (ρ_2) to reflect the fact that most of the time the immune system is working quickly when a person is infected (ρ_1). Because the virus is lethal, we use D a significant portion of the time, with varying percentages (ρ_3).

In each Figs. 6–8, we plotthe percentages of healthy (solid line), infected (small dashes), and dead or depleted (longer dashes) as a function of time in days. We also include output from the SCA itself; recall that only white coordinates represent healthy cells and all other colors show either infected or dead cells. The number of days is marked above each SCA frame. With ρ_2 temporarily fixed at 0 (not a very likely scenario, but a good control value), we vary ρ_1 and therefore $\rho_3 = 1 - \rho_1$. The different values of ρ_1 affect the timing of the recovery. We first show the output for $\rho_1 = 0.55$, $\rho_2 = 0$, and $\rho_3 = 0.45$; Fig. 6 illustrates Theorem 2.10, that with $\rho_2 = 0$ arbitrary runs of the model lead to full recovery, and using a much smaller value for ρ_3, say 0.1, reduces the infection and speeds up the recovery. This is shown in Fig. 8. Even if ρ_3 has a higher value (representing an infection in an organ that cannot repair itself quickly), when $\rho_2 = 0$, there will still be recovery, which can take place within the time frame of about 3 weeks.

We next introduce a strictly positive ρ_2 to represent a delay in the immune response time. Recall that ρ_2 corresponds to the rule L that causes the extra state to appear in the SCA, and only delays the transition to the state of healthy or dead by one time step. In Figs. 9–11 we show that the percentage of healthy cells decreases and the percentage of infected cells increases

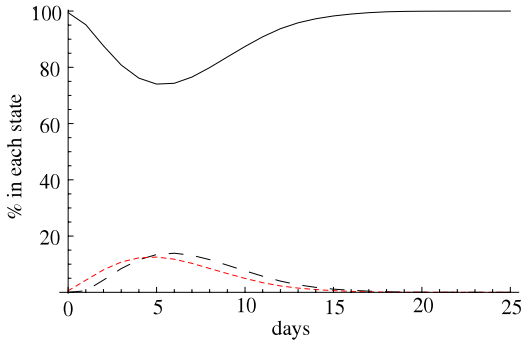

Fig. 8. Using $\rho_3 = 0.1$ for example, reduces the infection and improves recovery for almost every initial infection when $\rho_2 = 0$.

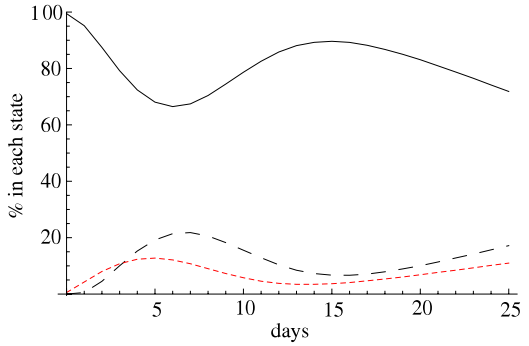

Fig. 9. If ρ_2 is very small but positive, (here $\rho_2 = 0.0005$, $\rho_3 = 0.45$) the likely outcome is the infection will persist and the percentage of healthy cells will decrease.

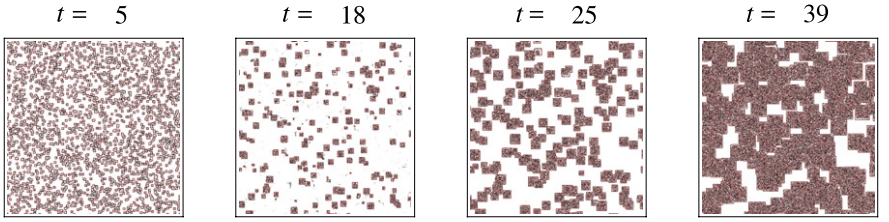

Fig. 10. This shows the SCA output using $\rho_2 = 0.0005$, $\rho_3 = 0.45$ as in Fig. 9.

over time, even for very small positive values of ρ_2. When ρ_2 is larger, we observe a faster transition to a limiting state and leads to the "terminal limit" which is probably not survivable (because the limits are close to 1/3). This is discussed in the next section and illustrated in Figs. 12 and 13.

3.2. Limiting percentages of healthy cells

Choosing the parameter $\rho_2 > 0$ corresponds to the event that the immune system does not clear out the virus immediately, and therefore not all initial infection points converge to the healthy state. Since up to now drugs have only intermittently been administered with success, often the infection persists, spreads throughout the organ, and the spatial rules no longer apply. We describe here the limiting proportions of healthy, infected, and dead cells that would occur in this model if no drug intervention occurred and if the patient's organ damage did not lead to a fatal outcome.

As discussed in Refs. [6,10], the virus dynamics are now ruled by the incidence matrix $B = B_{ij},\ i, j = 0, 1, \ldots, 3$, where $B_{ij} = 1$ if a cell can go from state i to state j in one time step, and 0 otherwise. The corresponding incidence matrix is given by:

$$B = \begin{pmatrix} 1 & 1 & 0 & 0 \\ 0 & 0 & 1 & 1 \\ 0 & 0 & 0 & 1 \\ 1 & 0 & 0 & 1 \end{pmatrix}. \tag{3.1}$$

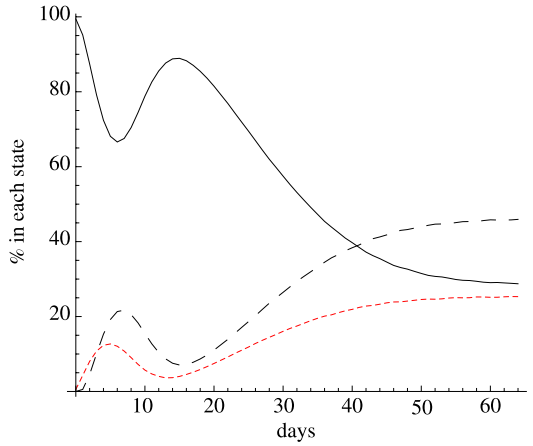

Fig. 11. If we run the model for a longer time than shown in Fig. 9 ($\rho_2 = 0.0005, \rho_3 = 0.45$) we see the healthy cells decrease towards a limit of around 27%.

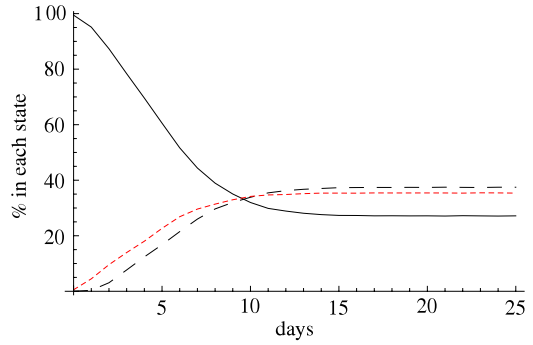

Fig. 12. Here, $\rho_2 = 0.35$, and $\rho_3 = 0.3$, and clearly the infection persists and the percentage of healthy cells decreases to a limiting value.

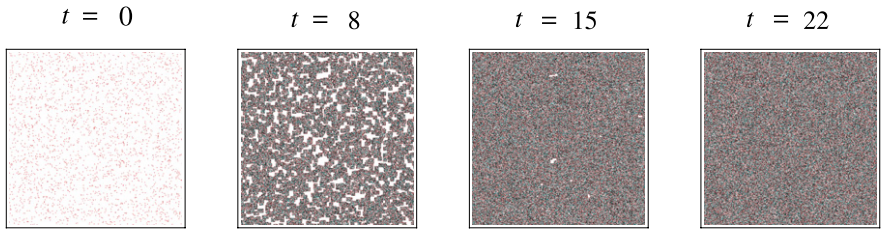

Fig. 13. The output of the SCA shows that when $\rho_2 = 0.35$ and $\rho_3 = 0.3$, clearly the infection persists and the percentage of healthy cells decreases to a low limiting value.

The matrix B defines a subshift (of finite type), $\Sigma_B \subseteq \mathcal{A}^{\mathbb{Z}}$, given by $\Sigma_B = \{a = \cdots a_0 a_1 \ldots \in \mathcal{A}^{\mathbb{Z}} : B_{a_i a_{i+1}} = 1\}$. The natural dynamical system to consider on Σ_B is a Markov shift σ, given by $\sigma(a)_j = a_{j+1}$, and we think of placing a Markov shift with the same incidence matrix B at every coordinate $(i, j) \in \mathbb{Z}^2$.

According to a classical theorem ([17] and see Proposition 3.2 below), described in detail in Refs. [6,10], this incidence matrix B gives rise to a shift invariant Markov probability measure ν on Σ_B defined as follows. There exist a probability vector $p = (p_0, p_1, p_2, p_3)$, with $p_k > 0$, and a 4×4 stochastic matrix $P = (p_{ij})_{i,j=0,\ldots,3}$ (i.e., $p_{ij} \geq 0$ and all row sums are 1), satisfying

$$pP = p. \tag{3.2}$$

From the pair (p, P) we define a measure ν on Σ_B by setting, for each finite sequence $c_0, c_1, \ldots, c_m$,

$$\nu(\{a \in \Sigma_B : a_k = c_k,\ k = 0, \ldots, m\}) = p_{c_0} \cdot p_{c_0 c_1} \cdots \cdot p_{c_{m-1} c_m}.$$

We call (σ, ν) the (p, P)-Markov shift, and note that it is invariant for σ on Σ_B.

The matrix P is obtained from B and from probabilities assigned by p_{ij} representing the probability of moving from state i to state j in one time step. We note that $p_{ij} > 0$ if and only if $b_{ij} = 1$, and for this model, we see that the correct form for P is:

$$P = \begin{pmatrix} \frac{1}{256} & \frac{255}{256} & 0 & 0 \\ 0 & 0 & \rho_2 & 1-\rho_2 \\ 0 & 0 & 0 & 1 \\ 1-\rho_3 & 0 & 0 & \rho_3 \end{pmatrix}. \tag{3.3}$$

The entry p_{11} comes from counting the proportion of 3×3 patterns with central coordinate 0 which have only 0s and 3s in the remaining eight coordinates. The entry p_{12} represents the rest of the patterns, which will update the central 0 to a 1. For this matrix P we can solve explicitly for the eigenvector p; in particular, it is not difficult to see that

$$v = \left(\frac{256}{255}(1-\rho_3),\, 1-\rho_3,\, \rho_2(1-\rho_3),\, 1\right) \tag{3.4}$$

satisfies $vP = v$, and the entries of v sum to $\alpha = 2 + \frac{256(1-\rho_3)}{255} + \rho_2(1-\rho_3) - \rho_3$. We then use the vector

$$p = \alpha^{-1}v = \frac{1-\rho_3}{\alpha}\left(\frac{256}{255},\, 1,\, \rho_2,\, \frac{1}{1-\rho_3}\right) \tag{3.5}$$

for the desired probability vector p which gives the invariant measure.

Remarks 3.1. (1) The vector p from Eq. (3.5) is the left eigenvector for the eigenvalue 1, normalized to be a probability vector. The entries p_k of p represent the probability that if we sample a cell randomly from the organ or compartment being modeled, then the cell will be in state $k \in \{0, 1, 2, 3\}$. Since only state 0 represents the healthy cells, p_0 is the proportion of healthy cells overall. The other entries of p represent proportions of infected or dead cells.
(2) The vectors in Eqs. (3.4) and (3.5) depend on both ρ_2 and ρ_3 (and hence implicitly on $\rho_1 = 1 - (\rho_2 + \rho_3)$).
(3) The first entry of p can be simplified to:

$$p_0 = \frac{256(-1+\rho_3)}{-766 + 255\rho_2(-1+\rho_3) + 511\rho_3}, \tag{3.6}$$

which is the limiting proportion of healthy cells.

Markov measures indicate expected long-term behavior of a dynamical system, as is shown in the next result. We write the n-fold product of the stochastic matrix P with itself as P^n. Assuming that $\rho_2, \rho_3 \in (0, 1)$, it is easy to check that $P^4 > 0$, so P is called *primitive* and the following result holds (see e.g., Ref. [17, Chapter 4]).

Proposition 3.2. *Let P be a primitive (stochastic) matrix. Then there exists a unique strictly positive probability vector, p, with $pP = p$, and for any probability vector q,*

$$\lim_{n\to\infty} qP^n = p.$$

The significance of Proposition 3.2 is that if no intervention takes place, no matter what the initial infection is (represented by the vector q), over time a slow acting immune response to the viral infection ($\rho_2 > 0$) causes the infection to progress to a limiting percentage of healthy cells in an affected organ. In Fig. 14 we show the graph of p_0 from Eq. (3.6), the limiting proportion of healthy cells, as a function of ρ_2 and ρ_3. We note that the proportion is typically between 0.25 and 0.33 for most relevant values of the parameters. This low percentage of healthy cells, 25%–33%, does not indicate a good survival rate for EBOV if the viral infection gets to the Markov stages.

4. Conclusions

Our results show that our model gives a robust simulation of the course of EBOV, with both survivors and non survivors, depending on the parameters chosen. While the timing of the spread of Ebola and HIV in an individual are drastically different, since the underlying mechanism for viral infection (cell-to-cell infection) and immune response are similar, small variations in the model can lead to realistic simulations. Since the extreme virulence of EBOV restricts the scope of clinical studies, our mathematical model of the disease can provide a valuable tool for continuing analysis of the virus dynamics.

Acknowledgments

The authors would like to thank Donna Molinek for assistance with the Mathematica programs used for this paper. The first author was a research visitor in the Mathematics Department of UNC Chapel Hill when most of this work was carried out and thanks them for their hospitality.

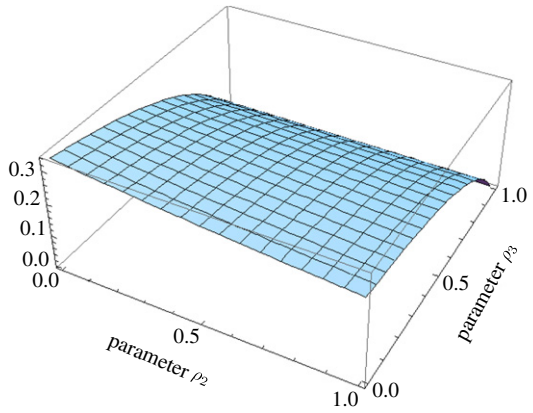

Fig. 14. The vector entry p_0, the limiting proportion of healthy cells, as a function of ρ_2 and ρ_3.

References

[1] M. Goeijenbier, et al., Ebola virus disease: a review on epidemiology, symptoms, treatment and pathogenesis, Neth. J. Med. 72 (9) (2014) 442–448.
[2] C.S. Powell, Shaking the Ebola tree: Genetic analysis offers insights into the workings of a notorious virus, Sci. Am. (1996) Retrieved from: http://www.scientificamerican.com/article/shaking-the-ebola-tree/.
[3] Y. Becker, Retrovirus and filovirus "immunosuppressive motif' and the evolution of virus pathogenicity in HIV-1, HIV-2, and Ebola viruses, Virus Genes 11 (2–3) (1996) 191–195.
[4] World Health Organization Ebola Response Team, Ebola virus disease in west africa - the first 9 months of the epidemic and forward projections, N. Engl. J. Med. 371 (16) (2014) 1481–1495.
[5] R.B. Martines, D.L. Ng, et al., Tissue and cellular tropism, pathology and pathogenesis of Ebola and Marburg viruses, J. Pathol. 235 (2) (2015) 153–174.
[6] E. Burkhead, J. Hawkins, D. Molinek, A dynamical study of a cellular automata model of the spread of HIV in a lymph node, Bull. Math. Biol. 71 (1) (2009) 25–74.
[7] R.M. Zorzenon dos Santos, S. Coutinho, Dynamics of HIV infection: A cellular automata approach, Phys. Rev. Lett. 87 (16) (2001) 168102-1–168102-4.
[8] R. Gonzalez, S. Coutinho, R. Zorzenon dos Santos, P. de Figueiredo, Dynamics of the HIV infection under antiretroviral therapy: a cellular automata approach, Physica A 392 (19) (2013) 4701–4716.
[9] R. Gonzalez, P. de Figueiredo, S. Coutinho, Cellular automata approach for the dynamics of HIV infection under antiretroviral therapies: the role of the virus diffusion, Physica A 392 (19) (2013) 4717–4725.
[10] J. Hawkins, D. Molinek, Markov cellular automata as models for chronic disease progression, Int. J. Biomath. (2015) http://dx.doi.org/10.1142/S1793524515500850. in press.
[11] J. Hawkins, Markov process models of the dynamics of HIV reservoirs under drug therapy. Preprint, 2015.
[12] S. Fink, Scientists trace Ebola's genetic path in Africa, weighing the role of mutations, N. Y. Times (2015) A6.
[13] A. Rambaut, D. Posada, et al., The causes and consequences of HIV evolution, Nature Rev. Genet. 5 (2004) 52–61.
[14] J. Towner, P. Rollin, et al., Rapid diagnosis of ebola hemorrhagic fever by reverse transcription-PCR in an outbreak setting and assessment of patient viral load as a predictor of outcome, J. Virol. 78 (8) (2004) 4330–4341.
[15] G.A. Hedlund, Endomorphisms and automorphisms of the shift dynamical system, Math. Syst. Theory 3 (4) (1969) 320–375.
[16] E. Gamber (Burkhead), Equicontinuity properties of *D*-dimensional cellular automata, Topology Proc. 30 (1) (2006) 197–222. Spring Topology and Dynamical Systems Conference.
[17] D. Lind, B. Marcus, An Introduction to Symbolic Dynamics and Coding, Cambridge Univ. Press, Cambridge, UK, 1995.